Supplementary Material (ESI) for Dalton Transactions
This journal is © The Royal Society of Chemistry

Three Multi-nuclear Clusters and One Infinite Chain Induced by Pendant 4-butyl-1H-pyrazole Ligand for Modification of Keggin Anions†

Ai-xiang Tian*, Ya-li Ning, Jun Ying, Xue Hou, Tian-jiao Li, Xiu-li Wang*

Department of Chemistry, Bohai University, Jinzhou 121000, People's Republic of China

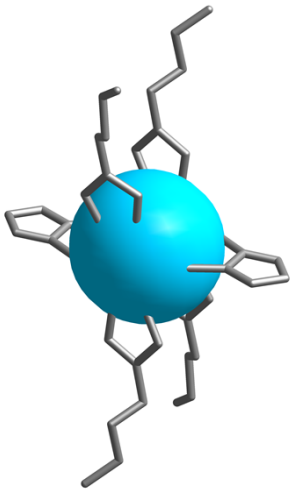

Fig. S1 The $[Cu^{I}_4(bpz)_4(pz)_2]^{2-}$ cluster in compound **1** with the bpz and pz molecules surrounding the Cu4 cores (blue sphere).

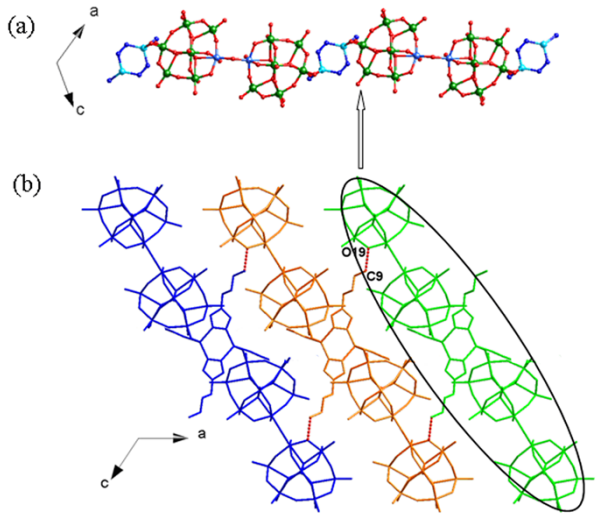

Fig. S2 (a) The 2D layer of compound **1** viewing along the *b* axis. (b) The 3D supramolecular structure of **1** through abundant hydrogen bonding interactions between adjacent layers, such as C9…O19 = 2.884 Å.

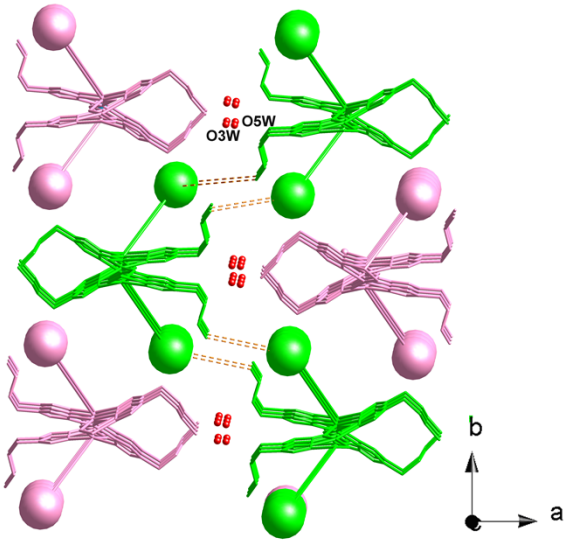

Fig. S3 The abundant hydrogen bonding interactions offered by crystal water molecules and $-(CH_2)_3CH_3$ groups to induce a 3D supramolecular structure of compound **2**.

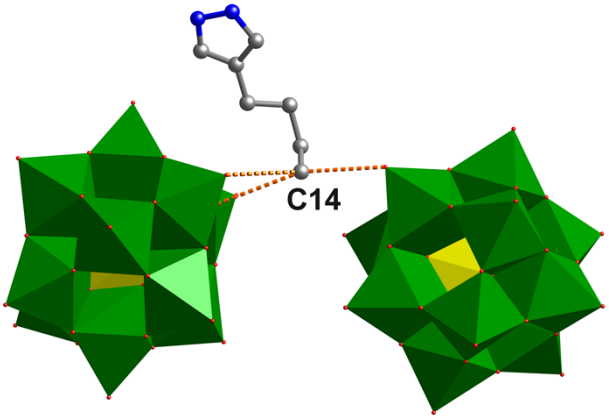

Fig. S4 The abundant hydrogen bonding interactions between bpz and anions of compound **3**, such as C14…O20 = 3.092 Å, C14…O38 = 3.129 Å, C14…O7 = 3.316 Å.

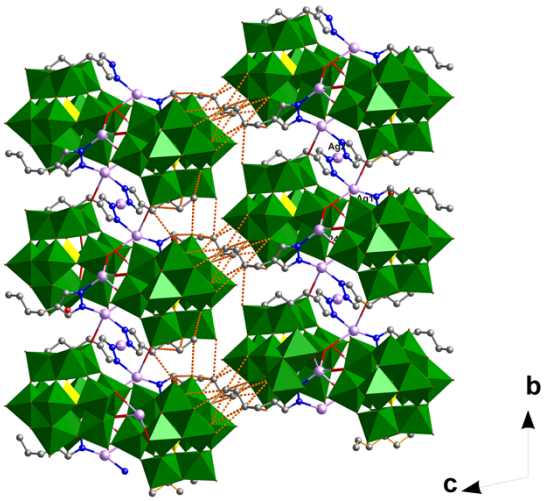

Fig. S5 The 3D supramolecular structure of compound **4** through hydrogen bonding interactions (orange dotted lines) supplied by $-(CH_2)_3CH_3$ and surface O atoms of anions to link adjacent layers.

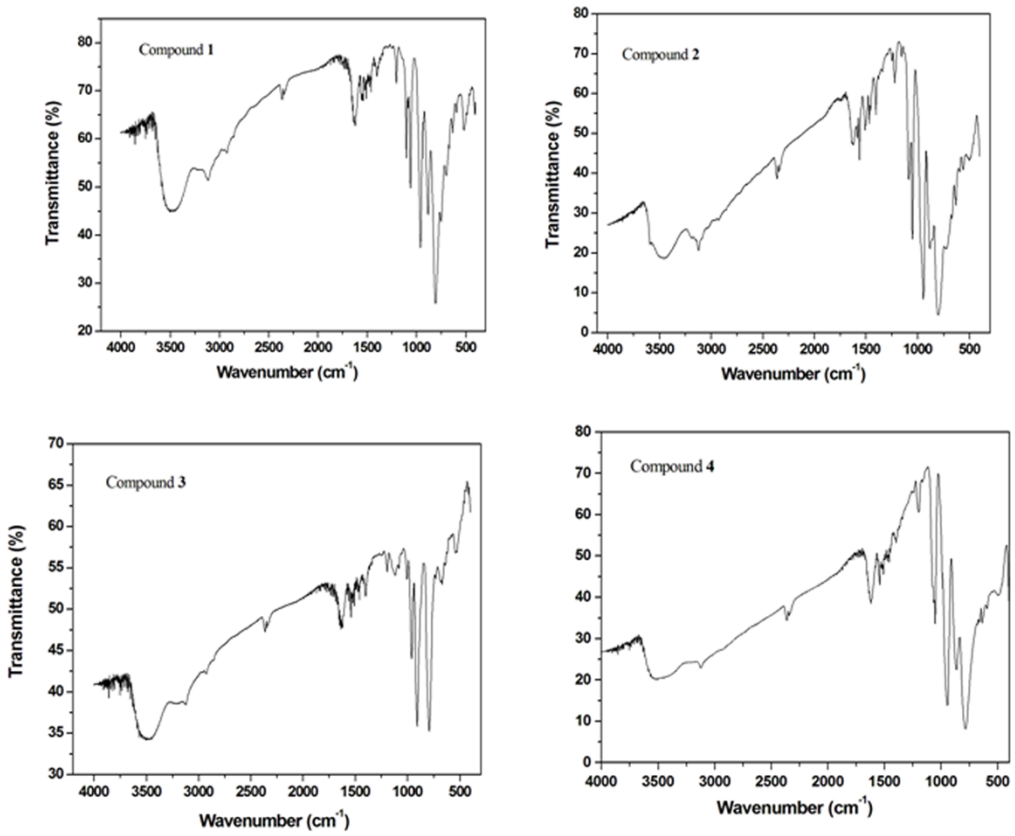

Fig. S6 The IR spectra of compounds **1–4**.

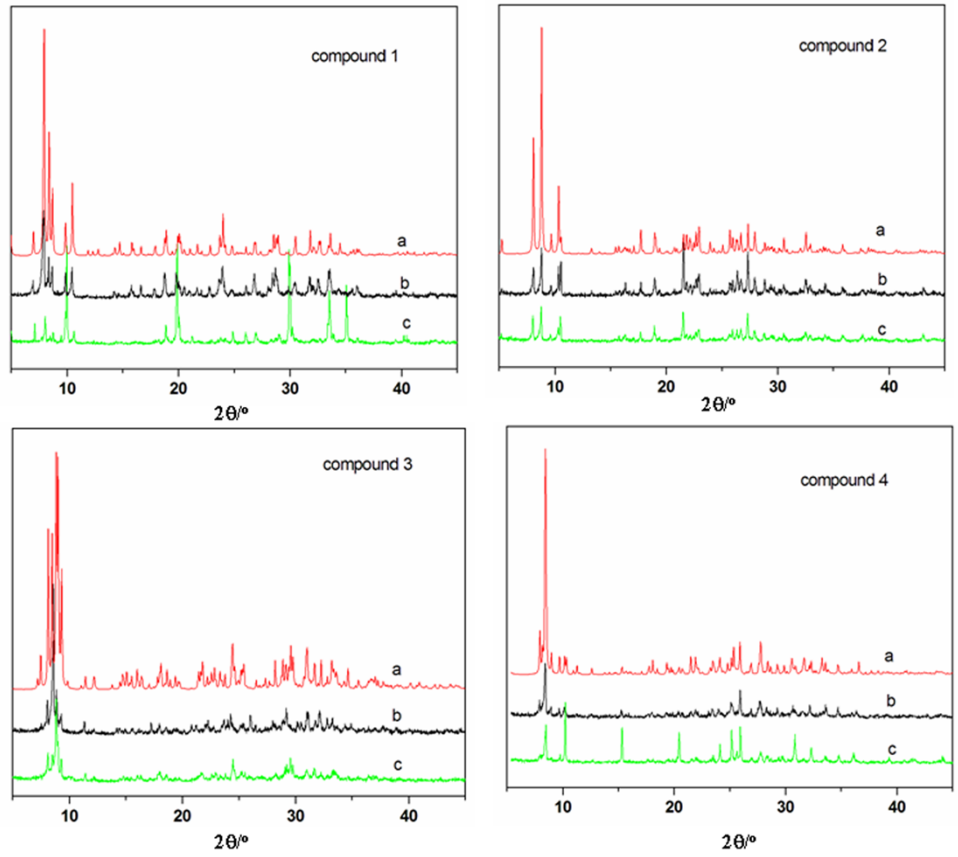

Fig. S7 The simulative (a), experimental (b) and recycled after photocatalysis (c) powder X-ray diffraction patterns for compounds **1**–**4**.

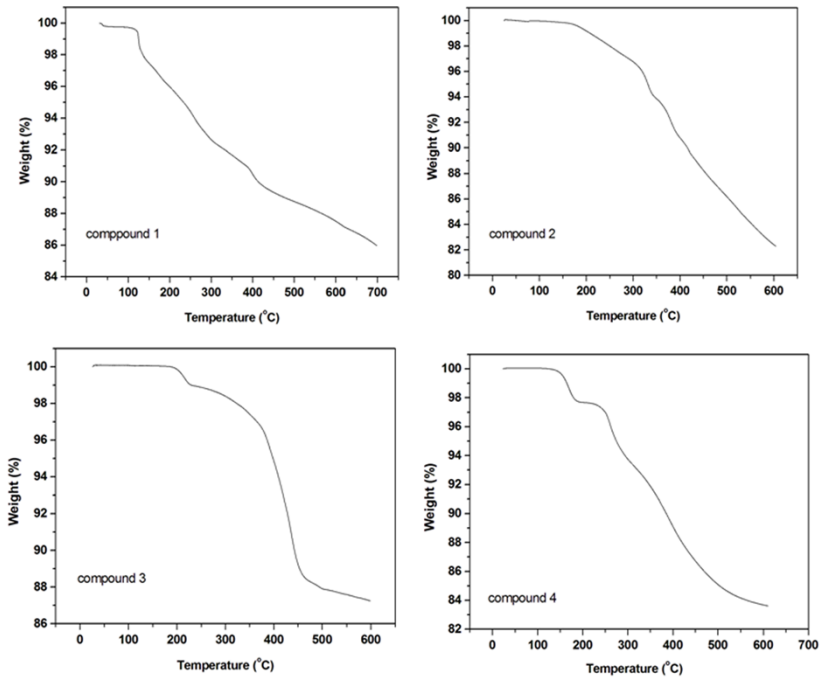

Fig. S8 The TG analyses of compounds **1**–**4**.

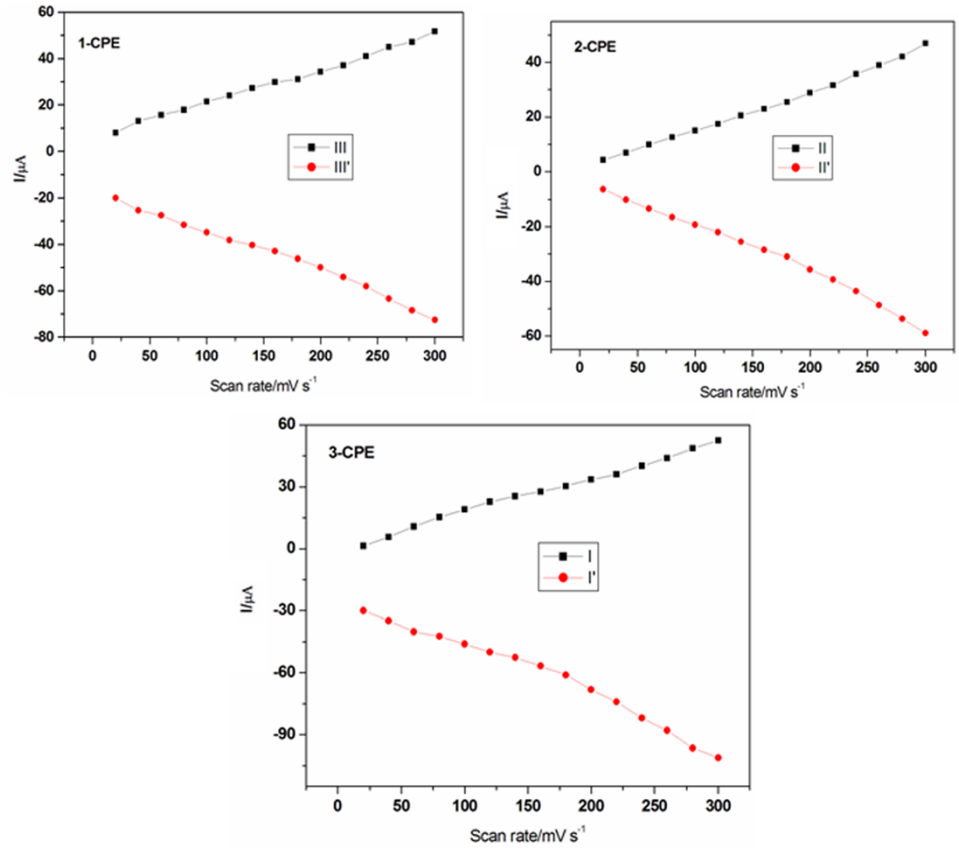

Fig. S9 The dependence of anodic peak and cathodic peak (III-III' for **1**–CPE, II-II' for **2**–CPE and I-I' for **3**–CPE) currents on scan rates.

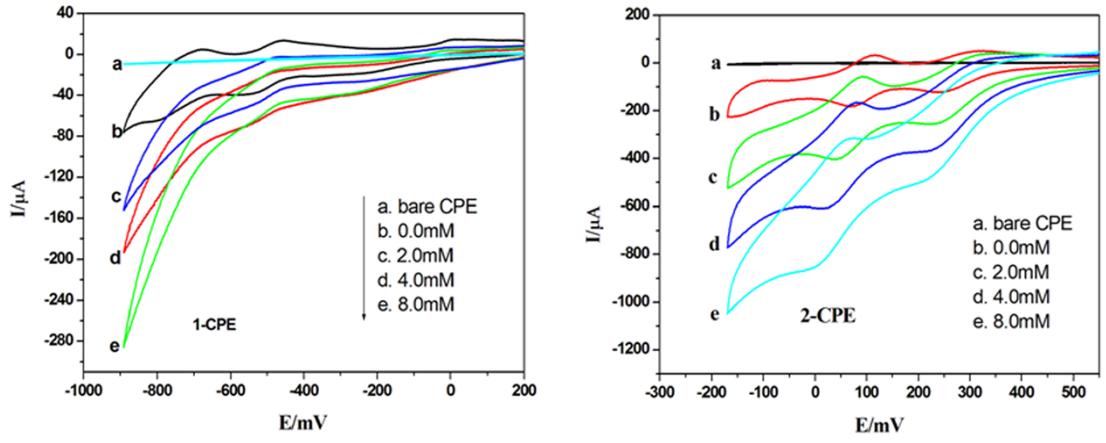

Fig. S10 Cyclic voltammograms of a bare CPE (a) and **1**–, **2**–CPEs in 0.1 M H_2SO_4 + 0.5 M Na_2SO_4 containing 0(b); 2.0(c); 4.0(d); 8.0(e) mM $NaNO_2$. Scan rate: 80 mV s^{-1}.

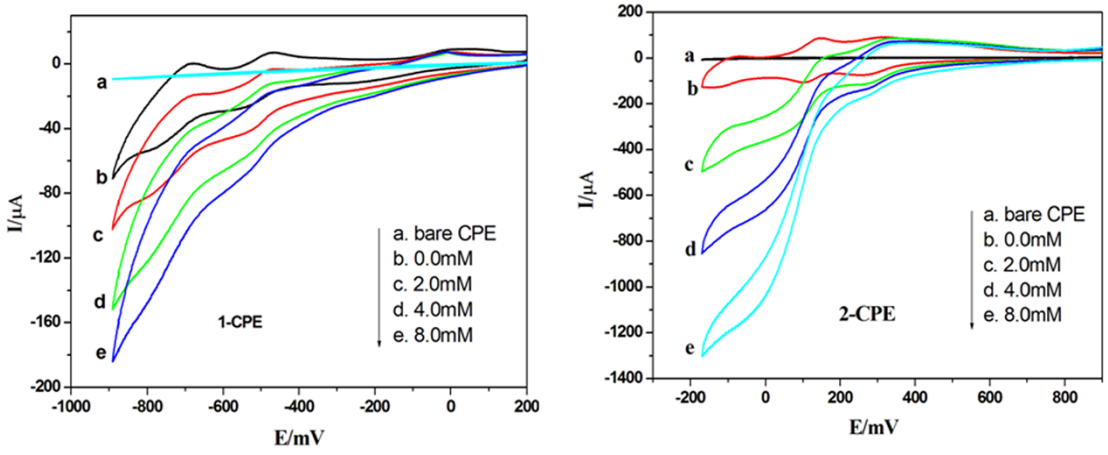

Fig. S11 Cyclic voltammograms of a bare CPE (a) and **1**–, **2**–CPEs in 0.1 M H_2SO_4 + 0.5 M Na_2SO_4 containing 0(b); 2.0(c); 4.0(d); 8.0(e) mM bromate. Scan rate: 80 mV s^{-1}.

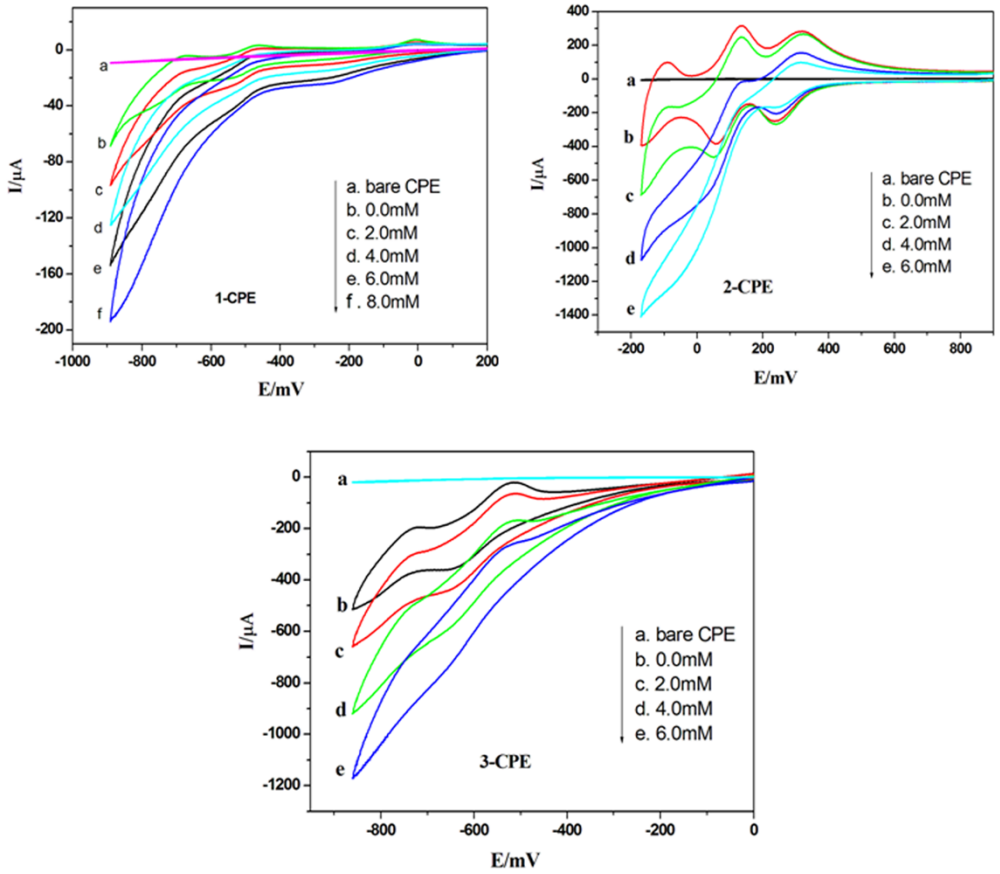

Fig. S12 Cyclic voltammograms of a bare CPE (a) and **1**–, **2**–CPEs in 0.1 M H_2SO_4 + 0.5 M Na_2SO_4 containing 0(b); 2.0(c); 4.0(d); 6.0(e); 8.0(f) mM H_2O_2. Scan rate: 80 mV s^{-1}.

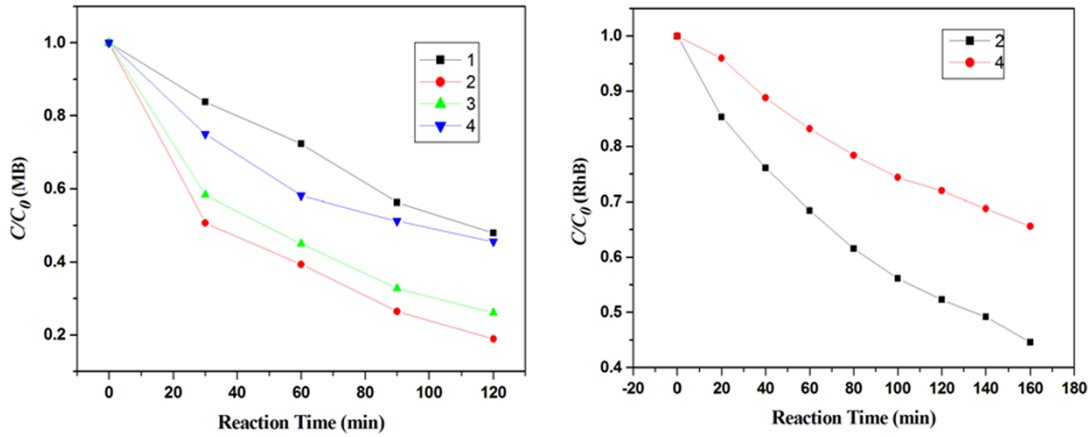

Fig. S13 Photocatalytic decomposition rate of the MB (left) and RhB (right) solution under UV irradiation with the use of the title compounds.

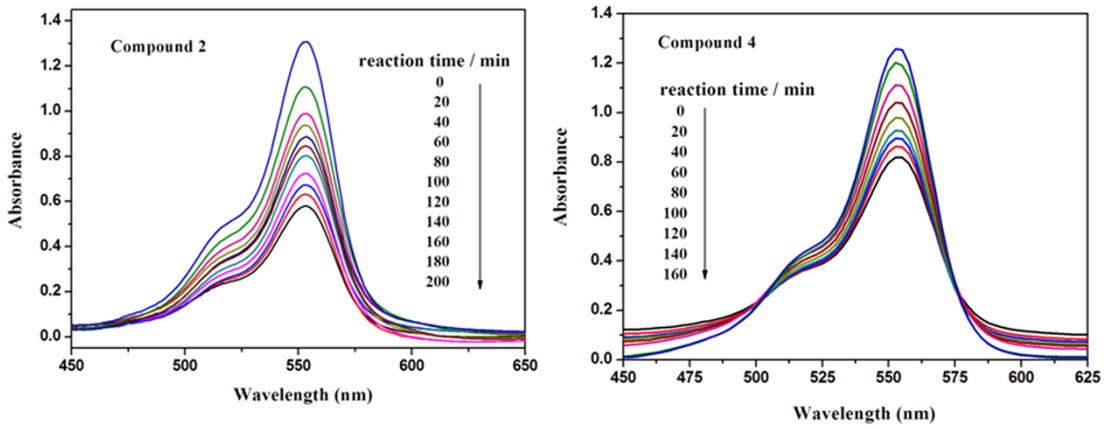

Fig. S14 Absorption spectra of the RhB solution during the decomposition reaction under UV irradiation with the presence of compounds **2** and **4**.

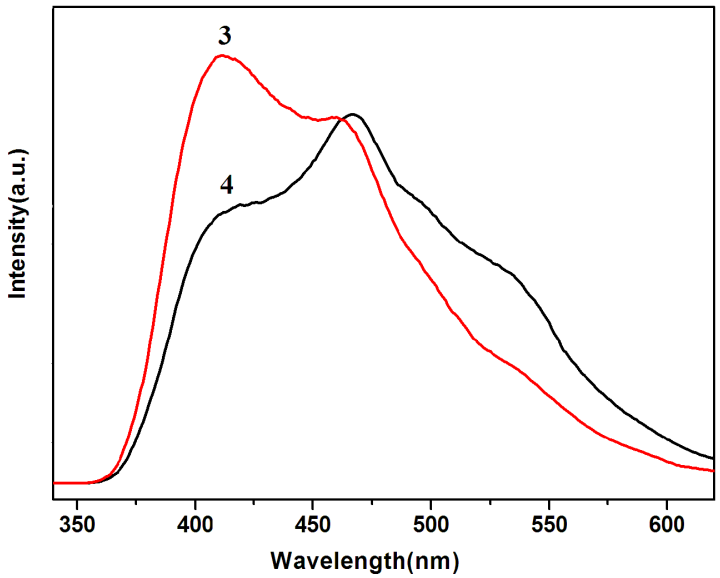

Fig. S15 The solid-state emission spectra of **3** and **4** at room temperature.

The solid-state photoluminescence spectra of **3** and **4** at room temperature are shown in Fig. S15. Two prominent emission peaks are observed at about 411 and 461 nm for **3** and 414 and 466 nm for **4** (excitation at 340 nm). The emission peak would be assigned to ligand-to-metal charge transfer (LMCT).

Table S1 Selected Bond Lengths (Å) and Bond Angles (°) for Compounds **1**–**4**.

Compound **1**			
Cu1-N2	1.952(5)	Cu1-N3	1.961(6)
Cu1-N1	2.008(7)	Cu1-O17	2.451(3)
Cu2-O7	1.948(5)	Cu2-O18	1.836(2)
Cu2-O19	1.961(5)	Cu2-O13	1.946(3)
Cu2-O14	2.018(4)	N2-Cu1-N3	130.0(3)
N2-Cu1-N1	113.1(3)	N3-Cu1-N1	112.7(2)
Compound **2**			
Cu1-O1W	1.902(4)	Cu1-O2W	1.910(4)
Cu1-N1	1.969(5)	Cu1-N3	1.980(5)
Cu2-O2W	1.903(4)	Cu2-O1W	1.909(4)
Cu2-N4	1.991(5)	Cu2-N2	1.986(5)
Cu2-O28	2.544(4)	O1W-Cu1-N1	88.95(18)
O1W-Cu1-O2W	169.1(2)	O2W-Cu1-N1	93.54(18)
O1W-Cu1-N3	92.30(19)	O2W-Cu1-N3	88.2(2)
N1-Cu1-N3	163.9(2)	O2W-Cu2-O1W	157.1(2)
O2W-Cu2-N4	87.38(17)	O1W-Cu2-N4	92.78(19)
O2W-Cu2-N2	97.14(17)	O1W-Cu2-N2	89.32(19)
N4-Cu2-N2	163.0(2)		

Compound **3**			
Ag1-N4	2.158(17)	Ag1-N1	2.183(19)
Ag1-Ag1	3.129(4)	Ag1-O3	2.774(5)
Ag1-O16	2.908(4)	Ag2-N2	2.170(19)
Ag2-N5	2.210(19)	Ag2-O13	2.677(4)
Ag2-O19	2.823(5)	Ag2-O15	2.855(4)
Ag3-N6	2.171(19)	Ag3-N3	2.14(2)
Ag3-O34	2.713(6)	Ag3-O13	2.621(4)
N4-Ag1-N1	165.6(8)	N4-Ag1-Ag1	113.4(5)
N1-Ag1-Ag1	79.5(6)	N2-Ag2-N5	168.6(8)
N3-Ag3-N6	171.8(8)		
Compound **4**			
Ag1-N3	2.128(6)	Ag1-N2	2.152(6)
Ag1-O18	2.850(5)	Ag2-N1	2.096(7)
Ag3-O6	2.459(5)	Ag3-N4	2.227(6)
Ag3-O24	2.523(5)	Ag3-O9	2.529(5)
Ag3-O8	2.721(6)	N1-Ag2-N1	179.999(3)
N3-Ag1-N2	159.0(2)	N4-Ag3-O6	113.56(18)
N4-Ag3-O24	140.72(18)	O6-Ag3-O24	105.13(15)
N4-Ag3-O9	109.12(18)	O6-Ag3-O9	82.05(17)
O24-Ag3-O9	82.09(16)		